

Design and Development of Gold/reduced Graphene Oxide Nanocomposite loaded with Cyclophosphamide: Potential Application in Treatment of Breast Cancer

Shaimaa Hassan Mallah¹, Ferdous Abbas Jabir^{2*}, Mohammed Abdulwahab Al-Askeri³

Abstract

Objective: Cyclophosphamide (CP) is a widely used anti-cancer drug. It works by alkylation and is commonly used in cancer treatment. In this study, the goal was to create biodegradable drug delivery carriers with minimal side effects for breast cancer treatment by developing gold nanoparticles/reduced graphene oxide (Au-rGO) nanocomposites using a sustainable synthesis method and loading them with cyclophosphamide. **Methods:** Cyclophosphamide-loaded gold/reduced graphene oxide nanocomposites (Au-rGO/CP) were synthesized and evaluated using FT-IR, XRD, release pattern, and FE-SEM techniques. Furthermore, the anticancer effect against breast cancer cells was evaluated through MTT and Annexin V assays. CAT, SOD, and GPx biomarkers were used to assess the antioxidant effect of the free and nano-formulated cyclophosphamide. **Results:** The characterization results showed the effective loading of cyclophosphamide in the nanocarriers. Additionally, Au-rGO had a higher drug loading capacity for cyclophosphamide during a 24-hour contact period (92.34%). The pH value affected the amount of cyclophosphamide released from the nanocarriers. Au-rGO/CP displayed significant in vitro anti-cancer activity against MCF-7 cancer cells relative to free CP and rGO/CP. According to Annexin V assay results, Au-rGO/CP induced a higher apoptosis rate in MCF-7 breast cancer cells than other forms. **Conclusion:** In conclusion, our findings demonstrate that the gold-decorated reduced graphene oxide nanocomposite enhances treatment efficacy and significantly increases apoptosis and cell death induction. As a result, CP-loaded Au-rGO-based compounds could be a promising treatment for breast cancer.

Keywords: Cyclophosphamide- drug delivery- graphene oxide- Gold Nanoparticles- breast cancer

Asian Pac J Cancer Prev, **25** (3), 1007-1016

Introduction

Breast cancer is the most frequently diagnosed malignant tumor in women globally and is also the primary cause of death from malignant tumors. Approximately 36% of all oncology patients are diagnosed with breast cancer [1, 2]. In 2018, an estimated 2.089 million women were diagnosed with breast cancer. The incidence of breast cancer is increasing worldwide, with the highest rates found in industrialized countries. Developed countries account for nearly half of all breast cancer cases globally. This increase in incidence is primarily attributed to the Western lifestyle, characterized by poor diet, smoking, excessive stress, and sedentary behavior. Despite advancements in diagnosis and treatment, the incidence of breast cancer continues to rise. This necessitates the exploration of new treatment methods, predictive factors, and prognosis [3]. Chemotherapy is a common treatment

strategy for cancer. Furthermore, direct injection of chemotherapeutic agents has limited antitumor efficacy and can lead to unfavorable adverse effects on healthy cells [4, 5]. Therefore, special attention has been given to designing carriers to improve drug delivery efficiency and minimize their adverse effects. The emergence of nanoscience has led to a new era in drug delivery systems (DDSs), with significant potential to address the limitations of classical chemotherapy, such as loading issues, poor distribution, and dosage-related adverse effects [6]. Various nanocarriers, including liposomes, polymeric nanomaterials, copolymer block micelles, and dendrimers, have significantly advanced scholarly fields due to their effective pharmacological effects, controlled release, and targeted delivery. The pharmaceuticals can be loaded through various mechanisms, such as embedding, hydrogen bonding interactions, and physical absorption [7-10]. Graphene, a two-dimensional planar

¹Chemistry Department, College of Science, University of Al-Qadisiyah / Al-Qadisiyah, Iraq. ²Medical Chemistry Department, College of Medicine, University of Al-Qadisiyah, Al-Qadisiyah, Iraq. ³College of Biotechnology, University of Al-Qadisiyah, Al-Qadisiyah, Iraq. *For Correspondence: Ferdous.alturaihy@qu.edu.iq

structural material, has a larger specific surface area than most other substances. It may generate significant hydrophobic interactions or π - π stacking and electrostatic interactions with the bioactive compounds, making it a suitable carrier for drug loading and cancer treatment [11]. Gold nanoparticles (AuNPs) are recognized as a significant functional component commonly used with other nanostructured materials [12, 13]. They are valued for their stability [14] and biocompatible properties, which enhance the selectivity of the entire composite [15]. As a result, the hybrid composite of graphene/AuNPs has attracted significant attention in cancer nano-therapy [16-20]. Cyclophosphamide (CP) is a phosphoramidate compound that acts as an antitumor agent and is widely used in the treatment of autoimmune diseases [21-24]. The cellular toxicity or tumor cell death induced by CP has been linked to the production of reactive oxygen species [23]. In both healthy and cancerous tissues, the activated CP metabolites are released, causing damage to cellular proteins, mitochondrial and lysosomal membranes, and DNA [25]. Combination therapy may be more effective than single medications in enhancing the efficacy of the diagnostic and therapeutic agent, as well as its biocompatibility. Therefore, the current study involved loading cyclophosphamide into gold nanoparticles/reduced graphene oxide (Au-rGO/CP). Hybrid materials enhanced with nanotechnology and synthesized from reduced graphene oxide (rGO) by decorating gold nanoparticles (AuNPs) for a drug delivery system are both labor- and cost-efficient.

Furthermore, biocompatible carbon materials can serve as a drug delivery system (DDS), delivering pharmaceutical molecules in nanoscale dimensions to provide targeted delivery of appropriate doses with reduced toxicity and adverse effects [26]. Nanocarriers can enhance pharmaceutical solubility and bioavailability, thereby increasing pharmaceutical loading on the surface.

In the present study, our aim was to design and develop cyclophosphamide-loaded gold/reduced graphene oxide (Au-rGO) nanocomposites. Furthermore, the toxicity and anticancer potential on MCF-7 cells were assessed using MTT and Annexin V assays. CAT, SOD, and GPx biomarkers were used to evaluate the antioxidant activity of both the free and nano-formulated CP.

Materials and Methods

Cyclophosphamide was purchased from Sigma-Aldrich. 3- "4,5-dimethylthiazolyl-2,5-diphenyltetrazolium bromide" (MTT) was obtained from Merck. Dimethyl sulfoxide (DMSO, 99.5%) and the DMEM (Dulbecco's Modified Eagle Medium) culture medium were obtained from Gibco-Invitrogen (Paisley, Scotland, UK). Propidium iodide (PI) and Annexin V-FITC were obtained from Sigma-Aldrich (St. Louis, MO, USA). CAT, SOD, and GPx assay kits were obtained from Bio-diagnostic Co., Ltd. The MCF-7 and HEK-293 cell lines were acquired from the Pasteur Institute in Tehran, Iran. All the chemicals were used without additional purification.

Synthesis of graphene oxide (GO)

In the present study graphene oxide (GO) was synthesized from pure graphite powder using a modified Hummers method [27].

Preparation of ginger extracts

Ginger roots were purchased from the local market and then washed frequently with distilled water. It was dried and powdered. Next, 5 grams of powder were mixed with 100 milliliters of distilled water and incubated for 3 hours at 50°C. The solution was filtered and stored at 4°C until it was used to synthesize rGO and Au-rGO nanomaterials [28].

Synthesis of reduced Graphene Oxide (rGO)

Reduced graphene oxide (rGO) was synthesized by mixing 15 milliliters of ginger extract with a 1 mg/mL GO suspension. The mixture was stirred using a mechanical stirrer at 80°C for six hours. The rGO was then collected by centrifugation at 8000 rpm for 10 minutes, rinsed five times with ultrapure water to remove ginger extract, and dried for two hours in a vacuum oven at 80 °C [29].

Synthesis of reduced Graphene Oxide decorated with gold (Au-rGO)

One-pot synthesis of Au-rGO nanocomposite was done with 0.5 mL of HAuCl₄.3H₂O (10 mg/mL), 100 mL of rGO suspension (1.5 mg/mL), and 5 mL of aqueous ginger extract (5%) and kept under magnetic stirring for 2 hours at 80°C. After two hours, the nanocomposite was centrifuged at 8000 rpm for 20 minutes, rinsed five times with distilled water, and dried in a vacuum oven at 80 °C [30].

Drug loading procedure

The gold-graphene nanocomposites (Au-rGO) and reduced graphene oxide (rGO) were loaded with chloramphenicol (CP) by immersing CP powder in 200 milliliters of PBS solution at pH 7.4 with varying concentrations of CP (2 milligrams to 20 milligrams) and incubating for 24 hours with vigorous mechanical stirring. The mixtures loaded with CP (Au-rGO/CP) and (rGO/CP) were collected by centrifugation, then repeatedly rinsed with PBS, and vacuum-dried at 25 °C. The centrifuged and washed solutions were collected, and the remaining amount of drug was calculated using ultraviolet-visible spectroscopy at 244 nm. The drug loading capacity of CP was assessed by creating a standard curve from the UV-Vis absorbance of CP standard solutions at different known concentrations.

The following equations were used to evaluate the loading capacity (LC) and loading efficiency (LE) of the CP:

$$LE \% = \frac{(\text{The initial amount of CP} - \text{Free CP})}{\text{The initial amount of CP}} \times 100\%$$

$$LC \% = \frac{(\text{The initial amount of CP} - \text{Free CP})}{\text{The amount of Au - rGO/CP}} \times 100\%$$

Drug release procedure

Five milligrams of the previously prepared CP-loaded Au-rGO or CP-loaded rGO powders were suspended in five milliliters of PBS solution with different pH values (5 and 7.4) and sealed in dialysis membranes (molecular weight cutoff = 3500) for drug release studies. At a constant temperature of 37°C with gentle stirring (100 rpm/min), the dialysis membranes were incubated in a 50-milliliter PBS solution with a comparable pH value. Five milliliters of the release media were replaced with fresh buffer solution at various time intervals (15, 30, 60, 120, 180, 240, 300, 360, 420, 480, and 720 minutes). The amount of CP released was calculated by measuring UV-Vis absorption at 244 nm.

The following equation was used to evaluate the concentrations of released CP from each interval:

$$\% \text{ Drug Release} = \frac{(W1)}{(Wt.)}$$

W1 represents the CP releasing weight, while Wt. represents the CP loading weight.

Biochemical Assays

Cell lysates

Cell lysates were prepared from cells treated with control, CP, rGO/CP, and Au-rGO/CP to detect oxidative stress biomarkers, including catalase (CAT), superoxide dismutase (SOD), and glutathione peroxidase (GPx). In summary, MCF-7 cells (1×10^6 cells/mL) were grown in the culture flask. When they reached a density of 80%, they were treated with CP, rGO/CP, and Au-rGO/CP. After 48 hours of treatment, the cells were detached and washed with cold PBS. Afterward, the pellet of cells was lysed in a cell lysis solution containing 150 mM NaCl, 120 mM Tris-HCl (pH 7.5), 1 mM Na₂EDTA, 2.5 mM sodium pyrophosphate, and 1% Triton. After centrifugation at 14,000 x g for 5 minutes at 4°C, the cell extracts were stored in the refrigerator for further analysis.

Determination of catalase activity

CAT test kits (Teb Pazhouhan Razi (TPR)) were used to measure the activity of catalase (CAT). To measure CAT activity, 30 µL of methanol, 100 µL of buffer solution, and 20 µL of hydrogen peroxide (H₂O₂) were mixed with 20 µL of the sample supernatant. The mixture was then incubated in a dark place on a shaker. After 20 minutes of incubation at room temperature, 30 µL of stop solution and 30 µL of chromogenic reagents were added to the samples and shaken in the dark. After a 10-minute incubation at 25°C, each sample was treated with 10 µL of an oxidizing reagent. The samples were placed in a covered petri dish and incubated at 25°C for 5 minutes. Finally, the average absorbance of each sample was measured at 540 nm using a microplate reader. One unit of CAT represents the amount of enzyme that decomposes 1 µmol of H₂O₂ per minute [31].

Determination of Superoxide Dismutase activity

The SOD assay kit (Teb Pazhouhan Razi, Tehran, Iran) was used to measure SOD activity after treating

cells with CP, rGO, AuNPs, Au-rGO, rGO/CP, AuNPs/CP, and Au-rGO/CP (each at its MTT IC₅₀) following the manufacturer's protocol. The absorbance of the samples was measured at 450 nm using a plate reader [32].

Determination of Glutathione peroxidase (GPx) activity

GSH is oxidized to GSSG in the presence of t-butyl hydroperoxide and GPx. This method is based on measuring the difference in absorbance values at 340 nm, which indicates the oxidation of NADPH to NADP⁺ in response to the reduction of GSH to GSSG by the GR enzyme. After adding all the chemicals to the sample, reference cuvettes were incubated at 37°C for 10 minutes. Next, the sample cuvette was filled with t-butyl hydroperoxide, and its activity was determined in comparison to the reference. One GPx unit represents the utilization of one microgram of GSH per minute [33].

Characterization techniques

An X-ray diffractometer (D/Max-2005, Rigaku) using Cu-K α radiation ($\lambda = 0.15405$ nm) and a scan rate of 3° (2 θ) per minute in the range of 2 $\theta = 5^\circ$ -80° was used to capture the X-ray diffraction patterns of the prepared materials. Fourier transform infrared (FT-IR) spectra of the samples were obtained using a PerkinElmer FT-IR spectrometer within the 4,000-400 cm⁻¹ range. Furthermore, the morphology of the nanomaterials was investigated using a field emission scanning electron microscope, specifically the ZEISS SIGMA VP FESEM.

Cell culture

MCF-7 and HEK-293 cell lines were bought from the Institute Pasteur (Tehran, Iran). Dulbecco's Modified Eagle's Medium (DMEM; Gibco, Life Technologies, Waltham, MA, USA) was used to culture the cells, supplemented with 10% FBS (BioWest SAS, Nuaille, France) and 1% penicillin/streptomycin (antibiotic antimycotic solution, Sigma-Aldrich®, St. Louis, MO, USA) in a humidified incubator with 5% CO₂ at 37°C.

In vitro cytotoxicity assay

The MTT (3-(4,5-dimethylthiazol-2-yl)-2,5-diphenyl tetrazolium bromide) method was employed to assess the cytotoxicity of the CP, rGO/CP, and Au-rGO/CP composites on the MCF-7 and HEK-293 cell lines [34]. Both cells were cultured in DMEM culture medium supplemented with 100 µg/mL of penicillin, 100 U/mL of streptomycin, and 10% FBS. Throughout the experiment, flasks were consistently kept in a humid environment, specifically at 37°C with a 5% carbon dioxide supply. MCF-7 and HEK-293 cells were seeded in a 96-well plate and incubated for 24 hours. Subsequently, they were treated with CP, rGO/CP, and Au-rGO/CP composites at various concentrations (500, 250, 125, 62.5, 31.25, 15.625 µg/mL) for 48 hours. After 48 hours, the exam medium was discarded and thoroughly rinsed with 1% phosphate-buffered saline (PBS). For 4 hours, the cells were incubated with 100 µL of MTT solution. Afterward, the supernatant was discarded, and the formazan crystals produced were dispersed in 100 µL of DMSO by shaking for 20 minutes. The plates were then read at 570 nm using

a microplate reader. The rate of absorption is directly proportional to the number of viable cells in the medium. Cell viability was defined as the percentage of treated cells' viability compared to that of untreated cells. The findings were presented as the average of three distinct tests. The concentrations of the samples that led to a 50% decrease in cell viability (i.e., I_{C50} values) were then estimated.

Apoptosis Assay (Annexin V-FITC/PI)

The apoptotic effect of the drugs was assessed using the Annexin V-FITC/PI staining method. The transfer of phosphatidylserine from the inner to the outer surface of phospholipids has been utilized to identify the apoptotic death of tumor cells. The observation can be made using an Annexin V (Annexin V-FITC) antibody, also referred to as a fluorescein isothiocyanate (FITC) dye [35]. Briefly, MCF-7 and HEK293 cells (5×10^4 cells per well) were seeded in 6-well plates and incubated for 24 hours. The medium is then withdrawn, and the cells are treated with CP, rGO/CP, and Au-rGO/CP at the I_{C50} concentration for 48 hours. Afterward, MCF-7 and HEK293 cells were separated and collected by centrifugation at 3000 rpm, followed by washing with cold phosphate-buffered saline. Then, 10 μ L of PI and 5 μ L of Annexin V-FITC were added and incubated for 15 minutes in the dark. Cell apoptosis was evaluated using flow cytometry.

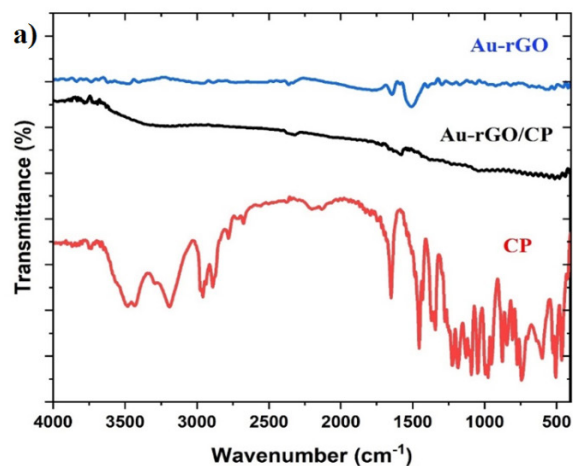
Statistical analysis

All experiments were conducted in triplicate, and the data presented are derived from a minimum of three independent experiments. Statistical analysis was conducted using GraphPad Prism 8, and the results were reported as mean \pm standard deviation. To assess statistical significance, paired t-tests and two-way ANOVA were conducted, and results with p-values less than 0.05 were deemed statistically significant.

Results

FT-IR Spectroscopy

FT-IR spectra were used to characterize the chemical



functional groups before and after the interactions (Figure 1a). The vibrational bands of Au-rGO are 3475.73 cm^{-1} , 1643 cm^{-1} , 1589.34 cm^{-1} , 1508 cm^{-1} , 1396 cm^{-1} , and 1296 cm^{-1} , belong to OH stretching, C=O stretching of carboxylic acid groups, aromatic C-C stretching, (C-OH) stretching, (C-O-C) stretching, and the C-O [36]. The FT-IR spectrum of CP demonstrates characteristic bands at 3433.29 cm^{-1} and 995.27 cm^{-1} for NH, and 1184.29 cm^{-1} for C-N stretching, with the wavenumber 1049.28 cm^{-1} indicating the O=P-OH group. (P=O) was associated with the peak at 1651.07 cm^{-1} . At 1342.46 cm^{-1} , the appearance of the -CH₂Cl bond was detected [37]. Au-rGO/CP possesses the characteristics of both materials. Moreover, the CP vibrational bands largely disappear, indicating a strong interaction with Au-rGO.

X-ray Diffraction (XRD) studies

The X-ray diffraction (XRD) technique was used to illustrate the crystal structures of Au-rGO and Au-rGO/CP. As shown in Figure 1b, the diffraction peaks of Au-rGO are observed at 38.2°, 44.4°, 64.63°, and 77.62°, representing index values of (111), (200), (220), and (311), verifying the crystalline face-centered cubic structure. When CP was loaded on Au-rGO, peaks were observed at 38.21°, 44.35°, 64.60°, and 77.66°. As indicated by XRD analysis, the lack of CP conjugation reaction effects on the size of Au-rGO cores suggests that the observed changes in nanoparticles can only be attributed to the expansion of their organic nanomaterial coating [38].

FE-SEM analysis

The surface morphologies of Au-rGO and Au-rGO/CP were examined using field emission scanning electron

Table 1. I_{C50} Concentration of CP, rGO/CP, and Au-rGO/CP Nanocomposites against Breast Cancer Cell Lines and Normal Cell Lines

Samples	MCF-7 I_{C50} ($\mu\text{g/mL}$)
CP	128.5
rGO/CP	103.36
Au-rGO/CP	74.92

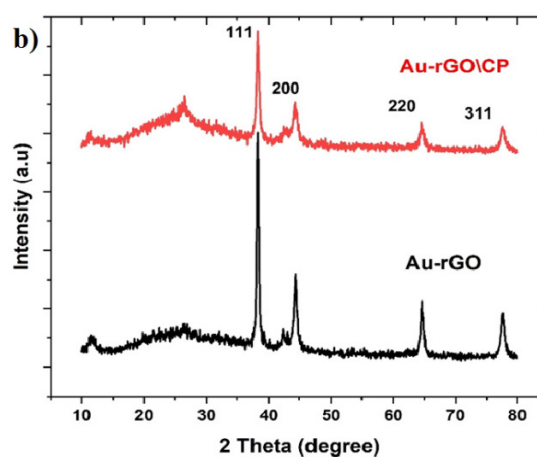


Figure 1. a) FTIR absorption spectra of Au-rGO, CP, and Au-rGO/CP. b) X-ray diffraction patterns of Au-rGO and Au-rGO/CP.

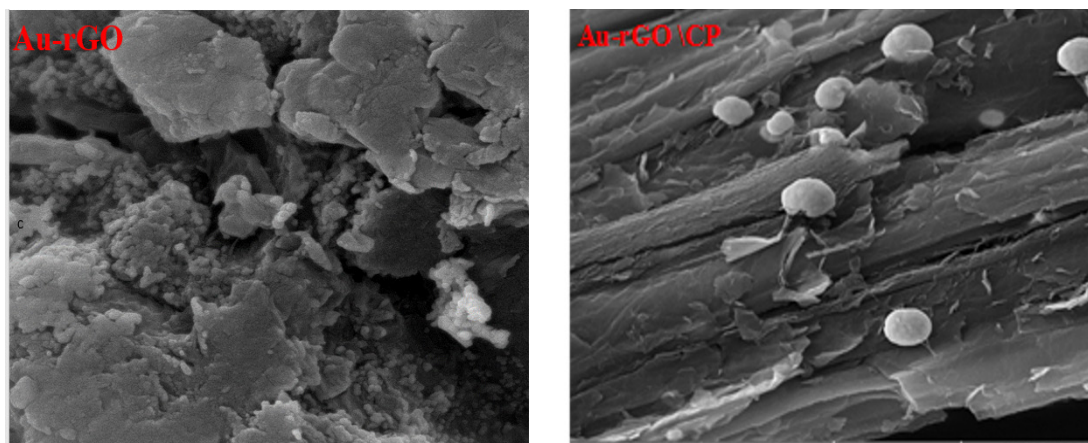


Figure 2. FE-SEM Images of Au-rGO and Au-rGO/CP

Table 2. Apoptotic (Annexin V/PI) Response towards rGO/CP, AuNPs/ CP, and Au-rGO/CP Compounds against Breast Cancer MCF7 and HEK293Cell Line

Apoptosis	Ann (-) PI (-) Healthy population	Ann (+) PI (-) Early apoptosis	Ann (+) PI (+) Late apoptosis	Ann (-) PI (+) Necrosis
MCF7 cell line				
Control	95.6	1.47	1.29	1.64
CP	46.4	8.89	17.5	27.2
rGO/ CP	74.14	11.64	9.5	4.72
Au-rGO/ CP	54.23	31.45	9.49	4.83
HEK293 cell line				
Control	94.5	1.86	0.443	3.24
CP	67.78	14.56	11.5	6.16
rGO/ CP	67	10.1	12.3	10.5
Au-rGO/ CP	59.94	28.37	8.73	2.96

microscopy (FESEM). The Au-rGO FESEM micrographs clearly show a spherical gold nanoparticle on the surface of the rGO sheets [39], and the surface appears smoother and more regular. The FESEM micrograph in Figure 2

depicts the unique shape of Au-rGO/CP. However, the surface of the Au-rGO/CP composite appears rough and irregular, likely due to the presence of the CP drug

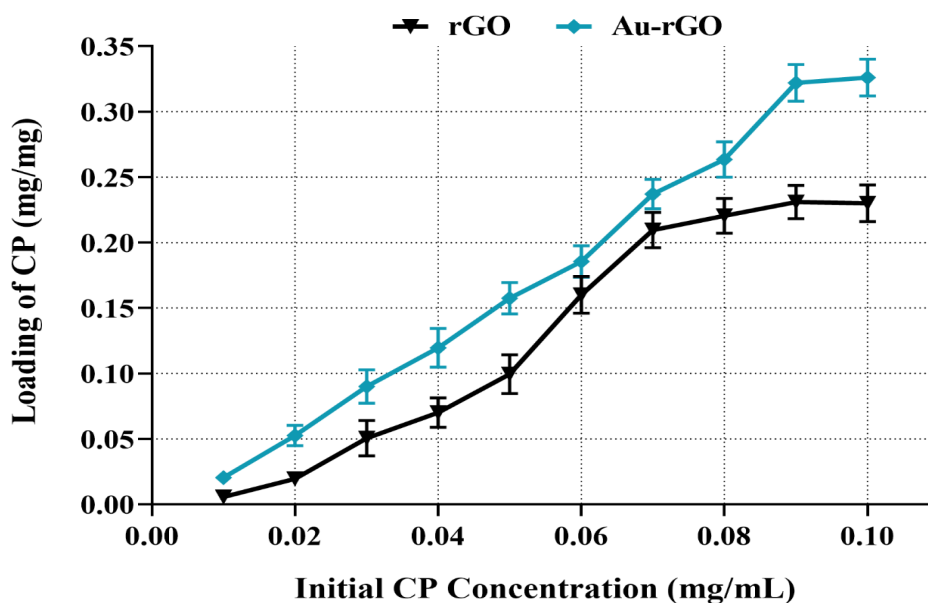


Figure 3. Drug Loading Capacity of rGO and Au-rGO at Different Initial CP Concentrations

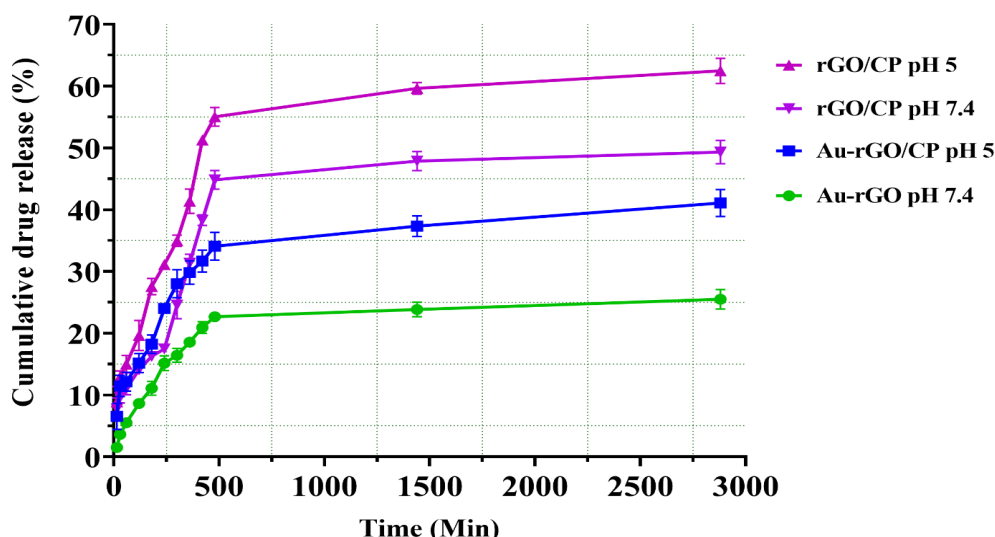


Figure 4. Cumulative Release from CP-loaded rGO and CP-loaded Au-rGO at Different pH Values.

Table 3. Catalase activity, inhibition ratio of SOD (%), and Glutathione peroxidase activity towards CP, rGO/CP, and Au-rGO/CP compounds against Breast Cancer MCF7 Cell Line

Samples	Catalase activity	The inhibition ratio of SOD (%)	Glutathione peroxidase activity
rGO/CP	25.83530572	26.26841244	355.2105263
Au-rGO/CP	2.112426036	30.11456628	449.4210526
CP	39.58284024	26.3502455	299.4210526
Control	18.96153846	20.04909984	257.8421053

Drug Loading and Release

The antitumor drug cyclophosphamide was utilized as a model to demonstrate the loading capacity and release pattern of rGO and Au-rGO nanocomposites. By comparing the original CP concentration solution with the supernatant solution after loading, the amount of chlorophyll a (CP)

loaded in reduced graphene oxide (rGO) and gold-reduced graphene oxide (Au-rGO) nanocomposites was estimated using their UV-Vis spectra at 244 nm. Figure 3 illustrates the loading capacity of reduced graphene oxide (rGO) and gold-reduced graphene oxide (Au-rGO) nanocomposites with CP in neutral conditions (pH 7.4). The results showed

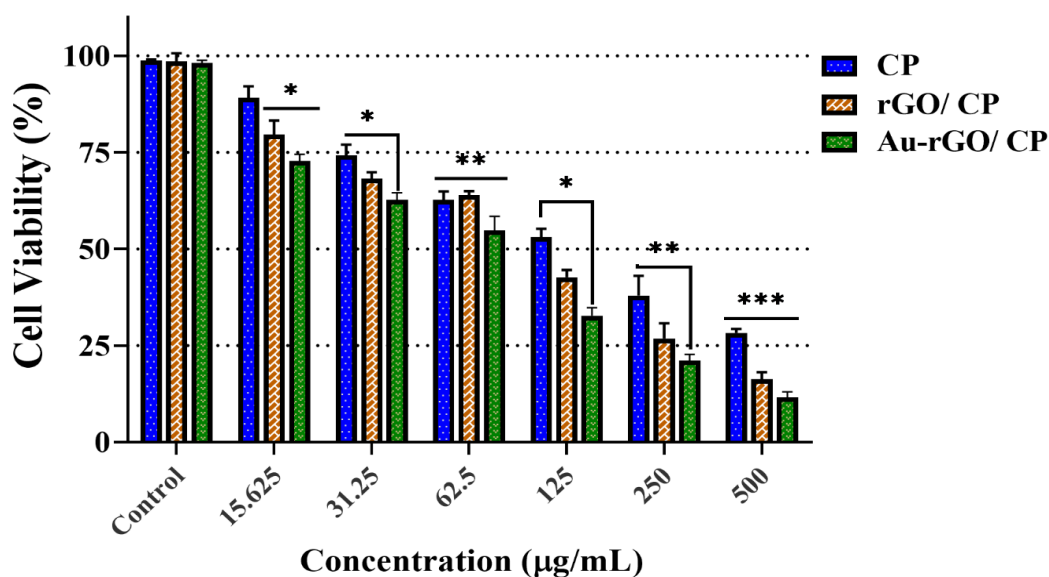


Figure 5. Cell Viability of MCF-7 Cell Line Cell Line after 48 h Treatment with CP, rGO/CP, and Au-rGO/CP. (***) p < 0.001, (**) p < 0.01, (*) p < 0.05).

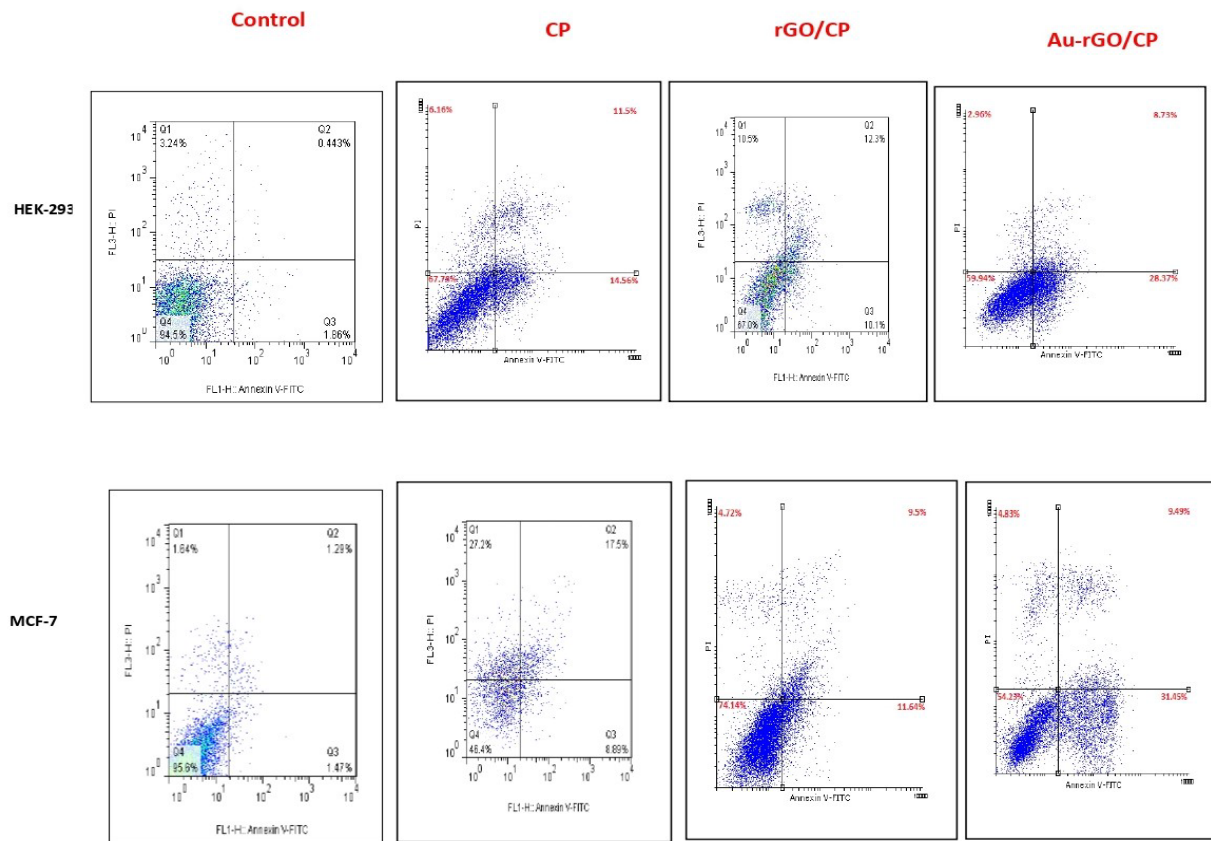


Figure 6. Annexin V-FITC Staining Results.

that Au-rGO nanocomposites are effective carriers for CP, with the highest loading efficiency of 92.34% after 24 hours. The saturated loading capacity of CP in the Au-rGO nanocomposite was 0.332 mg/mg, allowing for a maximum loading of 0.09 mg/mL of CP. The electrostatic interaction between the drug and gold nanoparticles makes Au-rGO a promising drug delivery system (DDS) for CP, with high drug loading and stability. FE-SEM morphology confirms that the AuNPs nanoparticles on the rGO sheet remain stable after drug loading (Figure 3). The electrical conductivity for reduced graphene oxide (rGO) was found to be 78.28 S/cm. The loading capacity (LC) of reduced graphene oxide (rGO) was 0.219 mg/mg, which was lower than that of the Au-rGO nanocomposite.

Figure 4 depicts the drug release profiles of rGO/CP and Au-rGO/CP at pH 7.4 (physiological pH) and 5.0 (cancer cell endosomal pH). The release profile of chlorophenol from Au-rGO/CP was significantly more prolonged than that from rGO/CP. After 24 hours, approximately 60% of chlorophenol (CP) was released from reduced graphene oxide/chlorophenol (rGO/CP) at pH 5.0, in contrast to only 42% from gold-reduced graphene oxide/chlorophenol (Au-rGO/CP). The pH value influenced the amount of CP released from the Au-rGO/CP. At pH 7.4, the release of CP was slower compared to the results at pH 5.0. For example, after 24 hours, approximately 42% of the CP was released at pH 5.0, while only 24% was released at pH 7.4. The pH-sensitive drug release behavior of the Au-rGO/CP was primarily due to the protonation of the amine group in the Au-rGO/CP in an acidic environment, leading to the cleavage of the

bonds between the CP and Au-rGO. Since most tumors have a lower pH than healthy tissues and tumor cells often have an acidic intracellular environment, the pH-sensitive drug release behavior of Au-rGO could be utilized in clinical applications for controlled drug delivery [40]. Due to the limited drug leakage from Au-rGO in normal physiological environments, the pH-sensitive controlled release behavior of Au-rGO/CP may be advantageous for targeting intracellular lysosomes and endosomes at low pH, enhancing cytotoxicity to tumor cells, while having a minimal effect on healthy cells. Previous studies have also found that chemotherapeutic drugs loaded onto Au-rGO are released more rapidly in acidic conditions compared to neutral conditions [41].

In vitro anticancer studies

The safety and toxic effects of nanoparticles are significant concerns in the medical and pharmaceutical fields. MTT assays were used to evaluate the cytotoxicity of CP, rGO/CP, and Au-rGO/CP on the MCF-7 cell line. Additionally, the safety of the synthesized NPs was assessed on HEK293 cell lines with treatment using blank rGO and Au-rGO (Figure 5). The MCF-7 cells were incubated with the agents at various concentrations (15.625, 31.25, 62.5, 125, 250, 500 $\mu\text{g/mL}$) for 48 hours. According to the MTT assay results, Au-rGO/CP exhibited higher dose-dependent cytotoxicity on MCF-7 breast cancer cells compared to free CP and rGO/CP. At lower concentrations, cyclophosphamide exhibits lower toxicity to MCF-7 cells. An increase in cyclophosphamide concentration from 15.625 to 500 $\mu\text{g/mL}$ reduces the

viability of MCF-7 cell lines from 77.79% to 10.48% (Figure 5). Furthermore, the incubation of HEK-293 cells showed no significant effect of the synthesized nanocomposite. The findings indicate that CP tagged with Au-rGO has a stronger anticancer effect than CP alone. The decrease in cell viability as nanoparticle concentration increases suggests the significant ability of nanoparticles to accumulate within the cells, causing stress and potentially leading to cell death. In Table 1, IC₅₀ values of the agents were summarized (concentration that reduced cell viability by half).

Discussion

The ability of free CP, rGO/CP, and Au-rGO/CP to induce apoptosis in MCF-7 cancer cells was analyzed using Annexin-V/PI staining [35]. The annexin V/PI apoptosis assay is a reliable method for determining the type of cell death by detecting phosphatidylserine on cell membranes. MCF7 and HEK-293 cell lines were treated with CP, rGO/CP, and Au-rGO/CP at IC₅₀ concentrations for 48 hours to examine the apoptotic effect (Figure 6). According to the findings in Table 2, Au-rGO/CP induced a higher rate of early apoptosis in human breast cancer cells compared to free CP and rGO/CP.

SOD, CAT, and GPx activities

SOD, CAT, and GPx are three important antioxidant biomarkers. Enzymatic antioxidants offer more effective protection against intense and extensive oxidative attacks because of their ability to decompose reactive oxygen species (ROS) [42]. Consequently, these antioxidants are crucial for combating inflammation, radiation damage, and acute hyperoxia damage. SOD acts as the first line of defense by converting the highly reactive superoxide anion (O₂^{•-}) to H₂O₂. Water and molecular oxygen are produced from the subsequent breakdown of H₂O₂ by catalase (CAT) [43]. Since glutathione peroxidase (GPx) is primarily responsible for eliminating hydroperoxides, it might prevent the oxidation of proteins, lipids, and membranes. The levels of glutathione peroxidase, superoxide dismutase, and catalase in MCF-7 cells were assessed to investigate the potential of nanoparticles to induce oxidative stress. Table 3 presents the levels of SOD, CAT, and GPx activity after 48 hours of treatment with CP, rGO/CP, and Au-rGO/CP on MCF-7 cells. SOD activity was significantly enhanced in the treated cells compared to the control at the IC₅₀ concentration for all samples. The induction of oxidative stress with H₂O₂ increased superoxide dismutase (SOD) activities. This can be explained by the cells' enzymatic antioxidant system adapting to reactive oxygen species (ROS) production [44]. As shown in Table 3, our results also demonstrated that the Au-rGO/CP exhibited the lowest CAT activity compared to the control and other samples. Regarding the significance of catalase (CAT) activity in cancer, studies have shown that inhibiting CAT activity can substantially elevate oxidative stress and hydrogen peroxide levels, leading to the death of cancer cells [45, 46]. According to Table 3, the treated cells exhibited significantly higher levels of GPx activity compared to the untreated control.

Again, Au-rGO/CP had significantly greater effects on antioxidant markers compared to pure CP and rGO/CP. The notable rise in GPx activity suggests that nanoparticles may stimulate the production of reactive oxygen species (ROS), leading to oxidative stress [47].

In conclusion, in this current investigation, we produced and analyzed cyclophosphamide-loaded gold /reduced graphene oxide (Au-rGO) nanocomposites with the aim of creating a biodegradable drug delivery vehicle that minimizes adverse effects for the treatment of breast cancer. The synthesized nanoparticles exhibited a sustained release profile, diminutive dimensions, high drug loading capacity, and robustness. Additionally, our research demonstrated that nanoparticle encapsulation of an antitumor agent enhances therapeutic efficacy and significantly augments the induction of apoptosis and cell death. Consequently, compounds based on CP-loaded Au-rGO hold potential as a promising approach for the treatment of breast cancer.

Author Contribution Statement

Shaimaa Hassan Mallah: Methodology, Investigation, Data curation, Original draft preparation. Mohammed Abdulwahab Al-Askeri: Methodology, Investigation, Data curation, Original draft preparation. Ferdous Abbas Jaber: Supervision, Conceptualization, Writing- Reviewing and Editing.

Acknowledgements

Availability of data and materials

The data and materials that support the findings of this study are available from the corresponding author, upon reasonable request.

References

- Nardin S, Mora E, Varughese FM, D'Avanzo F, Vachanam AR, Rossi V, et al. Breast cancer survivorship, quality of life, and late toxicities. *Front Oncol.* 2020;10:864. <https://doi.org/10.3389/fonc.2020.00864>.
- Bellanger M, Zeinomar N, Tehranifar P, Terry MB. Are global breast cancer incidence and mortality patterns related to country-specific economic development and prevention strategies? *J Glob Oncol.* 2018;4:1-16. <https://doi.org/10.1200/JGO.17.00207>.
- Smolarz B, Nowak AZ, Romanowicz H. Breast cancer-epidemiology, classification, pathogenesis and treatment (review of literature). *Cancers (Basel).* 2022;14(10):2569. <https://doi.org/10.3390/cancers14102569>.
- Amjad MT, Chidharla A, Kasi A. *Cancer chemotherapy.* 2020.
- Gorgzadeh A, Hheidari A, Ghanbarikondori P, Arastonejad M, Goki TG, Aria M, et al. Investigating the properties and cytotoxicity of cisplatin-loaded nano-polybutylcyanoacrylate on breast cancer cells. *Asian Pac J Cancer Biol.* 2023;8(4):345-50.
- Hare JI, Lammers T, Ashford MB, Puri S, Storm G, Barry ST. Challenges and strategies in anti-cancer nanomedicine development: An industry perspective. *Adv Drug Deliv Rev.* 2017;108:25-38. <https://doi.org/10.1016/j.addr.2016.04.025>.
- Hadi ZA, Odda AH, Jawad AF, Al-Tu'ma FJ. Design and development of fe₃o₄@ prussian blue nanocomposite:

- Potential application in the detoxification of bilirubin. *Asian Pac J Cancer Prev.* 2023;24(8):2809.
8. Abd-Rabou AA, KhM AZ, Kishita MS, Shalby AB, Ezzo MI. Nano-micelle of moringa oleifera seed oil triggers mitochondrial cancer cell apoptosis. *Asian Pac J Cancer Prev.* 2016;17(11):4929-33. <https://doi.org/10.22034/APJCP.2016.17.11.4929>.
 9. Harishchandra BD, Pappuswamy M, Antony P, Shama G, Pragatheesh A, Arumugam VA, et al. Copper nanoparticles: A review on synthesis, characterization and applications. *Asian Pac J Cancer Biol.* 2020;5(4):201-10.
 10. Abbasi M, Reihanisaransari R, Poustchi F, Hheidari A, Ghanbarikondori P, Salehi H, et al. Toxicity of carboplatin-niosomal nanoparticles in a brain cancer cell line. *Asian Pac J Cancer Prev.* 2023;24(11):3985-91. <https://doi.org/10.31557/APJCP.2023.24.11.3985>.
 11. Rashki S, Alshamsi HA, Amiri O, Safardoust-Hojaghan H, Salavati-Niasari M, Nazari-Alam A, et al. Eco-friendly green synthesis of znO/gqD nanocomposites using protoparmeliopsis muralis extract for their antibacterial and antibiofilm activity. *J Mol Liq.* 2021;335:116195. <https://doi.org/10.1016/j.molliq.2021.116195>
 12. Shochah QR, Jabir FA. Green synthesis of Au/ZnO nanoparticles for anticancer activity and oxidative stress against MCF-7 cell lines. *Biomass Conversion and Biorefinery.* 2023 Jan 6:1-4. <https://doi.org/10.1007/s13399-022-03697-2>
 13. Abdulhusain ZH, Alshamsi HA, Salavati-Niasari M. Facile synthesis of au/znO/rGO nanohybrids using 1, 8-diamino-3, 6-dioxaoctan as novel functional agent for photo-degradation water treatment. *Journal of Materials Research and Technology.* 2021;15:6098-112. <https://doi.org/10.1016/j.jmrt.2021.11.038>
 14. Alshamsil HA, Nema QA, Alwan SH. Facile one-step synthesis of Au-ZnO/MWCNTs for photocatalytic treatment of Reactive Blue dye in aqueous solution. In IOP conference series: earth and environmental science 2022 May 1 (Vol. 1029, No. 1, p. 012003). IOP Publishing.
 15. Gnanakani PE, Santhanam P, Premkumar K, Eswar Kumar K, Dhanaraju MD. Nannochloropsis extract-mediated synthesis of biogenic silver nanoparticles, characterization and in vitro assessment of antimicrobial, antioxidant and cytotoxic activities. *Asian Pac J Cancer Prev.* 2019;20(8):2353-64. <https://doi.org/10.31557/APJCP.2019.20.8.2353>.
 16. Song J, Yang X, Jacobson O, Lin L, Huang P, Niu G, et al. Sequential drug release and enhanced photothermal and photoacoustic effect of hybrid reduced graphene oxide-loaded ultrasmall gold nanorod vesicles for cancer therapy. *ACS Nano.* 2015;9(9):9199-209. <https://doi.org/10.1021/acsnano.5b03804>.
 17. Wang X, Han Q, Yu N, Li J, Yang L, Yang R, et al. Aptamer-conjugated graphene oxide-gold nanocomposites for targeted chemo-photothermal therapy of cancer cells. *J Mater Chem B.* 2015;3(19):4036-42. <https://doi.org/10.1039/c5tb00134j>.
 18. Xu C, Yang D, Mei L, Li Q, Zhu H, Wang T. Targeting chemophotothermal therapy of hepatoma by gold nanorods/graphene oxide core/shell nanocomposites. *ACS Appl Mater Interfaces.* 2013;5(24):12911-20. <https://doi.org/10.1021/am404714w>.
 19. Yuan Y, Zhang Y, Liu B, Wu H, Kang Y, Li M, et al. The effects of multifunctional mir-122-loaded graphene-gold composites on drug-resistant liver cancer. *J Nanobiotechnology.* 2015;13:12. <https://doi.org/10.1186/s12951-015-0070-z>.
 20. Loutfy SA, Salaheldin TA, Ramadan MA, Farroh Kh Y, Abdallah ZF, Youssef T. Synthesis, characterization and cytotoxic evaluation of graphene oxide nanosheets: In vitro liver cancer model. *Asian Pac J Cancer Prev.* 2017;18(4):955-61. <https://doi.org/10.22034/APJCP.2017.18.4.955>.
 21. Elshater AA, Haridy MAM, Salman MMA, Fayyad AS, Hammad S. Fullerene c(60) nanoparticles ameliorated cyclophosphamide-induced acute hepatotoxicity in rats. *Biomed Pharmacother.* 2018;97:53-9. <https://doi.org/10.1016/j.biopha.2017.10.134>.
 22. Shariatinia Z, Javeri N, Shekarriz S. Flame retardant cotton fibers produced using novel synthesized halogen-free phosphoramidate nanoparticles. *Carbohydr Polym.* 2015;118:183-98. <https://doi.org/10.1016/j.carbpol.2014.11.039>.
 23. Shariatinia Z, Shekarriz S, Mousavi HSM, Maghsoudi N, Nikfar Z. Disperse dyeing and antibacterial properties of nylon and wool fibers using two novel nanosized copper (ii) complexes bearing phosphoramidate ligands. *Arabian Journal of Chemistry.* 2017;10(7):944-55.
 24. Khan A, Aldebasi YH, Alsuhaibani SA, Khan MA. Thymoquinone augments cyclophosphamide-mediated inhibition of cell proliferation in breast cancer cells. *Asian Pac J Cancer Prev.* 2019;20(4):1153-60. <https://doi.org/10.31557/APJCP.2019.20.4.1153>.
 25. Shariatinia Z. Bonding of phosphoramidates onto b-c59 nanostructure as drug delivery systems. *Phys Chem Res.* 2018;6(1):15-29. <https://doi.org/10.22036/PCR.2017.89125.1389>
 26. Ivanova N, Gugleva V, Dobрева M, Pehlivanov I, Stefanov S, Andonova V. Silver nanoparticles as multi-functional drug delivery systems. London, UK: IntechOpen; 2018 Nov 5.
 27. Khalil WA, Sherif HHA, Hemdan BA, Khalil SKH, Hotaby WE. Biocompatibility enhancement of graphene oxide-silver nanocomposite by functionalisation with polyvinylpyrrolidone. *IET Nanobiotechnol.* 2019;13(8):816-23. <https://doi.org/10.1049/iet-nbt.2018.5321>.
 28. Yadi M, Azizi M, Dianat-Moghadam H, Akbarzadeh A, Abyadeh M, Milani M. Antibacterial activity of green gold and silver nanoparticles using ginger root extract. *Bioprocess Biosyst Eng.* 2022;45(12):1905-17. <https://doi.org/10.1007/s00449-022-02780-2>.
 29. Yang J, Xia X, He K, Zhang M, Qin S, Luo M, et al. Green synthesis of reduced graphene oxide (rGO) using the plant extract of salvia spinosa and evaluation of photothermal effect on pancreatic cancer cells. *J Mol Struct.* 2021;1245:131064.
 30. Zou M, Zhu H, Wang P, Bao S, Du M, Zhang M. Synthesis and characterization of Au nanoparticles/reduced graphene oxide nanocomposite: A facile and eco-friendly approach. *NANO.* 2014;9(03):1450031.
 31. Dogan S, Ozcan T, Dogan M, Turhan Y. The effects on antioxidant enzymes of pmma/hydroxyapatite nanocomposites/composites. *Enzyme Microb Technol.* 2020;142:109676. <https://doi.org/10.1016/j.enzmictec.2020.109676>.
 32. Barbasz A, Ocwieja M, Roman M. Toxicity of silver nanoparticles towards tumoral human cell lines u-937 and hl-60. *Colloids Surf B Biointerfaces.* 2017;156:397-404. <https://doi.org/10.1016/j.colsurfb.2017.05.027>.
 33. Fernandes E, Fonseca TG, Carrico T, Mestre N, Tavares A, Bebianno MJ. Cytotoxic responses of the anticancer drug cyclophosphamide in the mussel mytilus galloprovincialis and comparative sensitivity with human cells lines. *Chemosphere.* 2020;261:127678. <https://doi.org/10.1016/j.chemosphere.2020.127678>.
 34. Li R, Ji Z, Chang CH, Dunphy DR, Cai X, Meng H, et al. Surface interactions with compartmentalized cellular phosphates explain rare earth oxide nanoparticle hazard and provide opportunities for safer design. *ACS Nano.* 2014;8(2):1771-83. <https://doi.org/10.1021/nn406166n>.
 35. Lakshmanan I, Batra SK. Protocol for apoptosis assay by

- flow cytometry using annexin v staining method. *Bio Protoc.* 2013;3(6):e374-e. <https://doi.org/10.21769/bioprotoc.374>.
36. Abdulhusain ZH, Alshamsi HA, Salavati-Niasari M. Silver and zinc oxide decorated on reduced graphene oxide: Simple synthesis of a ternary heterojunction nanocomposite as an effective visible-active photocatalyst. *Int J Hydrogen Energy.* 2022;47(80):34036-47. <https://doi.org/10.1016/j.ijhydene.2022.08.018>
 37. Shah PV, Rajput SJ. A comparative in vitro release study of raloxifene encapsulated ordered mcm-41 and mcm-48 nanoparticles: A dissolution kinetics study in simulated and biorelevant media. *J Drug Deliv Sci Technol.* 2017;41:31-44.
 38. Wójcik M, Lewandowski W, Król M, Pawłowski K, Mieczkowski J, Lechowski R, et al. Enhancing anti-tumor efficacy of doxorubicin by non-covalent conjugation to gold nanoparticles–in vitro studies on feline fibrosarcoma cell lines. *PLoS One.* 2015;10(4):e0124955.
 39. Mukherjee S, Sushma V, Patra S, Barui AK, Bhadra MP, Sreedhar B, et al. Green chemistry approach for the synthesis and stabilization of biocompatible gold nanoparticles and their potential applications in cancer therapy. *Nanotechnology.* 2012;23(45):455103. <https://doi.org/10.1088/0957-4484/23/45/455103>.
 40. Joshi AS, Singh P, Mijakovic I. Interactions of gold and silver nanoparticles with bacterial biofilms: Molecular interactions behind inhibition and resistance. *Int J Mol Sci.* 2020;21(20):7658. <https://doi.org/10.3390/ijms21207658>.
 41. Depan D, Shah J, Misra R. Controlled release of drug from folate-decorated and graphene mediated drug delivery system: Synthesis, loading efficiency, and drug release response. *Mater Sci Eng C.* 2011;31(7):1305-12.
 42. Christofidou-Solomidou M, Muzykantov VR. Antioxidant strategies in respiratory medicine. *Treat Respir Med.* 2006;5(1):47-78. <https://doi.org/10.2165/00151829-200605010-00004>.
 43. Hasanuzzaman M, Bhuyan M, Zulfiqar F, Raza A, Mohsin SM, Mahmud JA, et al. Reactive oxygen species and antioxidant defense in plants under abiotic stress: Revisiting the crucial role of a universal defense regulator. *Antioxidants (Basel).* 2020;9(8):681. <https://doi.org/10.3390/antiox9080681>.
 44. Sznarkowska A, Kostecka A, Meller K, Bielawski KP. Inhibition of cancer antioxidant defense by natural compounds. *Oncotarget.* 2017;8(9):15996-6016. <https://doi.org/10.18632/oncotarget.13723>.
 45. Ott M, Gogvadze V, Orrenius S, Zhivotovsky B. Mitochondria, oxidative stress and cell death. *Apoptosis.* 2007;12(5):913-22. <https://doi.org/10.1007/s10495-007-0756-2>.
 46. Abbas YJ, Al-Tu'ma FJ, Al-Hemerri AF. Association between matrix metalloproteinase-2 gene variants and pathogenesis of breast cancer in sera of iraqi women. *J Contemp Med Sci.* 2020;6:285-90.
 47. Yuan YG, Zhang S, Hwang JY, Kong IK. Silver nanoparticles potentiates cytotoxicity and apoptotic potential of camptothecin in human cervical cancer cells. *Oxid Med Cell Longev.* 2018;2018:6121328. <https://doi.org/10.1155/2018/6121328>.



This work is licensed under a Creative Commons Attribution-Non Commercial 4.0 International License.